JOURNAL OF GEOPHYSICAL RESEARCH, VOL. 101, NO. B4, PAGES 8383–8392, APRIL 10, 1996

Modeling earthquake cycles in the Shumagin subduction segment, Alaska, with seismic and geodetic constraints

Gutuan Zheng, Renata Dmowska, and James R. Rice

Division of Applied Sciences, and Department of Earth and Planetary Sciences
Harvard University, Cambridge, Massachusetts

Abstract. Deformation associated with the earthquake cycle in the Shumagin Islands segment of the Alaska-Aleutian subduction zone is analyzed with the use of a two-dimensional finite element model. The model consists of an oceanic plate dipping under an upper plate, both of which respond elastically to stress fluctuations in the earthquake cycle, and these are underlain by asthenospheric mantle and mantle wedge regions which respond viscoelastically. It is tailored to the geometry of the Shumagin Islands region, by using seismicity to define the position of the interplate interface and (partially) coupled region along it. The model is preconditioned by forcing this interface to undergo periodically repeated slips up to (and including) the time of the May 31, 1917, event (M_s = 7.4) in that region, with each chosen to be consistent with the moment and estimated rupture area of that event. We investigated the dependence of model results for geodetic signals on the strength of seismic coupling between the plates and viscoelastic relaxation of deviatoric stresses in the mantle, including in the mantle wedge close to the plate junction and along the aseismic downdip continuation of the thrust interface. In models with significant relaxation in the wedge or downdip thrust zone, results show that as the intraseismic stage matures, there is a region of diminished compressional strain rates, and even of locally extensional rates, on the Earth's surface above the downdip end of the seismically coupled zone. Based on the seismic estimates of the location of the coupled zone, this region is in the area of the Shumagin Islands. We find that if approximately 20% of the convergence takes place seismically (compatible with the previous seismic history), and if an extensive region of relaxed deviatoric stress is assumed to be present in the wedge and/or along the downdip interface, then deformations predicted by the model can be made consistent with the measured strain data from the Shumagin Islands geodetic network [*Lisowski et al.*, 1988; *Larson and Lisowski*, 1994], as well as uplift and tilt data [*Savage and Plafker*, 1991; *Beavan*, 1992]. Our model simulations here suggest that the Shumagin segment is capable of large earthquakes. The hypothesis of totally aseismic subduction is not similarly consistent with all geodetic constraints.

Introduction

The Shumagin Islands subduction segment has been identified as a seismic gap between the 1938 earthquake (M_w = 8.2) to the east and the 1946 earthquake (M_s = 7.3) to the west [*Kelleher*, 1970; *Davies et al.*, 1981]. The eastern part of the Shumagin gap is shown in Figure 1. The area exhibits a variable mode of rupture. Previous large or great earthquakes which ruptured that part include July 22, 1788, April 16, 1847 [e.g., *Estabrook et al.*, 1994], and the most recent event of May 31, 1917 (M_s = 7.4, M_o = 1.7 × 10^{20} N m [*Estabrook and Boyd*, 1992]). Based on these 59- and 70-year intervals, an average repeat time of 65 ± 10 years has been estimated [*Nishenko*, 1991]. As of 1995 was 78 years since the last event. The accumulated seismic moment release rate of shallow (0-50 km depth) earthquakes in this area increases markedly, and much faster than linearly with time, since approximately 1980, which may reflect maturing of a locked gap [e.g., *Sykes and Jaumé*, 1990; *Dmowska and Lovison-Golob*, 1991; *Jaumé and Estabrook*, 1992; *Bufe et al.*, 1994]. The most recent event, continuing the trend of accelerated moment release that had already been reported, is the M_s = 6.9, M_o = 0.2-0.3 × 10^{20} N m event of May 13, 1993 [*Lu et al.*, 1994; *Tanioka et al.*, 1994]. Also, since 1977, there has been a cessation of the previously abundant, generally tensional, outer-rise seismicity [*Dmowska and Lovison-Golob*, 1991]. We have interpreted this as a sign that significant thrust zone coupling is decreasing the extensional stresses in the outer rise as the seismic cycle matures [*Dmowska et al.*, 1988]. Both these signs would suggest maturity of this segment. However, strain measurements as first reported based on electronic distance measurement (EDM) data for 1980-1987 from a network on the Shumagin Islands (Figures 1 and 2) seemed to not show any significant strain accumulation, suggesting that aseismic slip is occurring [*Lisowski et al.*, 1988] with negligible coupling. Subsequent Global Positioning System (GPS) data for 1987-1991 [*Larson and Lisowski*, 1994], combined with EDM data, showed a somewhat stronger indication of strain accumulation, with a trench-perpendicular compression rate of 0.026 ± 0.012 μstrain/yr averaged over the network. Also, the uplift data and tilt data [*Beavan*, 1992] do suggest observable variation that might

Paper number 95JB03461
0148-0227/96/95JB-03461$05.00

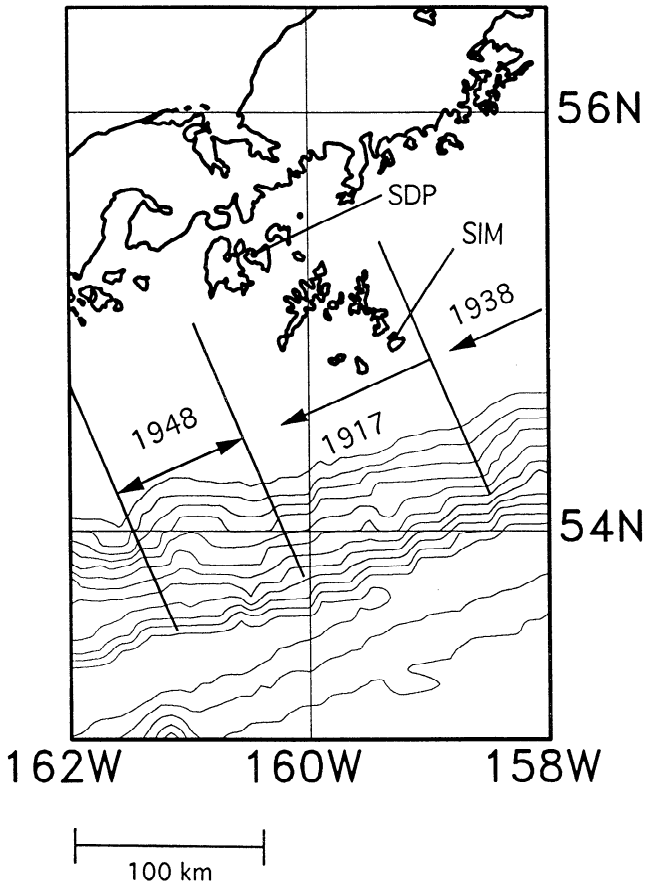

Figure 1. Map of Shumagin Islands region, Alaska, with along-arc rupture extents of the most recent large earthquakes shown (adapted from *Estabrook and Boyd* [1992]), and positions of Simeon (SIM) and Sand Point (SDP) geodetic stations marked. This area coincides with the eastern side of the Shumagin gap which, according to Estabrook and Boyd, extends another 75 km beyond the western edge of the 1948 zone shown.

be related to a seismically coupled subduction zone. With these observations in mind, we pose the following question: Given the seismic and geodetic constraints, can we judge if and how much the Shumagin segment is seismically coupled, and if at all coupled, what magnitude earthquake might be expected there in the future?

Rice and Stuart [1989] and *Taylor et al.* [this issue] investigated stressing during the earthquake cycle using the finite element method for a simple two-dimensional (2-D) model. With a viscoelastic mantle wedge of relatively short Maxwell (relaxation) time included in the modeling, they found an area of late-cycle extensional straining on the Earth's surface, above the downdip end of the locked zone. Instead, compressional straining dominates there in a purely elastic model or viscoelastic model with long Maxwell time. This observation suggested a possible way that the measured strains in the Shumagin Islands region could be small even in the presence of strong coupling. In this paper we tailor their 2-D model to the geometry of the Shumagin Islands region. The position of the interplate interface and possible locked region along it, especially relative to the Shumagin Islands geodetic network, is constrained by seismicity [*Beavan et al.*, 1984; *Hauksson* 1985; *Abers*, 1992]. We refine the finite element mesh as well, to systematically investigate the stress transfers and surface deformation during the earthquake cycle. Our simulations show that the location of the interplate interface and the viscosity of the upper mantle, especially of the downdip continuation of the interplate interface and the mantle wedge, are the most important parameters that control the cycle-related stressing and deformation in coupled subduction zones.

Deformation Observations

Surface strain data are reported by *Lisowski et al.* [1988] and *Larson and Lisowski* [1994]. The trilateration survey (EDM) for the 1980-1987 interval gave a very small trench-perpendicular extensional strain rate, averaged over the network. This was originally reported by *Lisowski et al.* [1988] as an extensional strain rate of 0.00 ± 0.03 μstrain/yr, with possible fluctuations within the network of the same order as the uncertainty or larger. A subsequent analysis of EDM data for that period by *Larson and Lisowski* [1994] was reported as −0.020 ± 0.015 μstrain/yr. *Larson and Lisowski* [1994] also analyzed GPS data for 1987-1991 and reported an average strain rate of −0.025 ± 0.025 μstrain/yr. Further, based on their combined analysis of both data sets, EDM and GPS, for the 11-year period 1980-1991, they report a "marginally significant" average strain

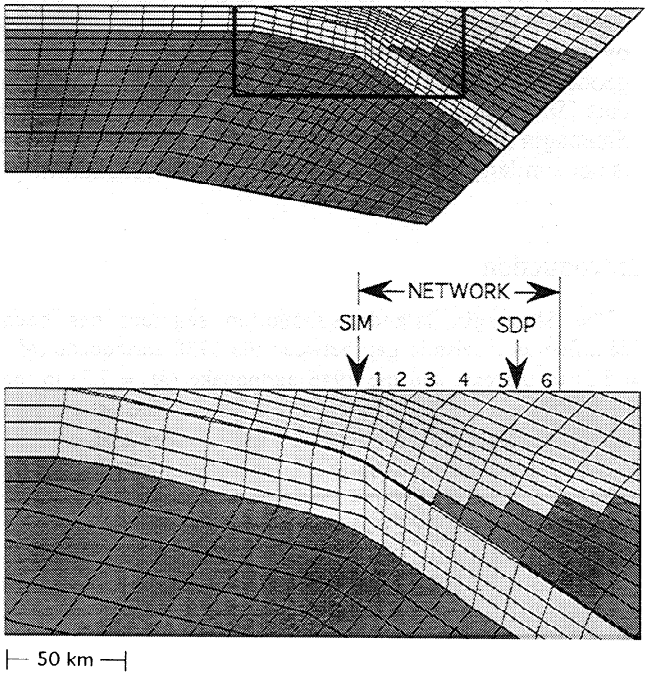

Figure 2. (Top) Finite element mesh. (Bottom) Expanded view of the rectangle marked above showing the extent of the geodetic network and geodetic stations Simeon (SIM) and Sand Point (SDP). The interplate fault zone corresponds to the thin layer of elements, of which the darkened part is the seismically coupled zone. The white part updip is aseismic. The white part downdip is an aseismic continuation with strong relaxation of deviatoric stresses in the first group of models considered. Element numbers are shown for surface elements within the geodetic network.

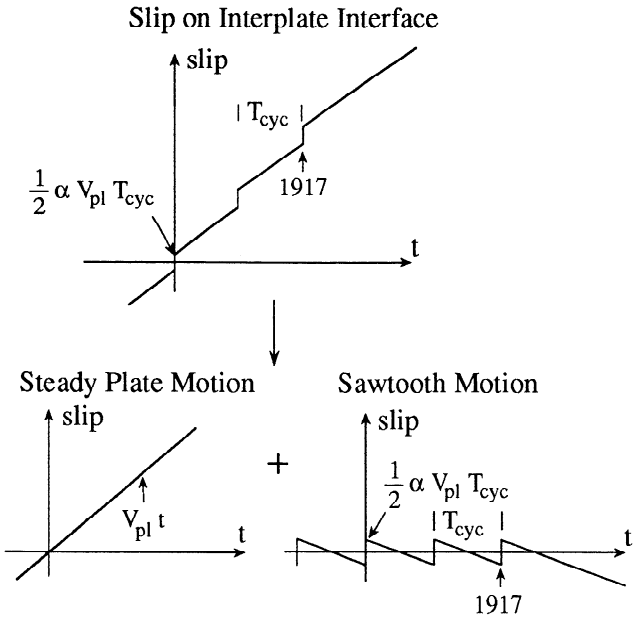

Figure 3. Decomposition of slip on the coupled part of the plate interface into steady slip and a sawtooth variation representing the slip perturbation due to earthquake cycles. Time dependence of deformation rates in the overlying plate is determined solely by the response to the sawtooth.

rate of –0.026 ± 0.012 μstrain/yr. They also showed [*Larson and Lisowski,* 1994, Figure 3] a trench-perpendicular velocity distribution along their 105-km-long network that suggested a very low compression rate over the central 60 to 70 km of the network, with a strong increase in strain rate in the part of the network nearest to the trench, and a milder increase in the part farthest from the trench. *Lisowski et al.* [1988] used an elastic dislocation model [*Savage,* 1983] of a fully coupled subduction zone to predict the trench-perpendicular strain rates. They found that the average value over the network is 0.19 μstrain/yr if only the shallow part of interplate interface is locked, and 0.17 μstrain/yr if the part of interplate interface which is locked extends further down to 50 km in depth. Since the small observed average strain rate is much lower than the predicted values, *Lisowski et al.* [1988] suggested the Shumagins segment is not coupled, at least in recent years. *Hudnut and Taber* [1987] argued on the basis of intermediate-depth seismicity that the western part of the Shumagin gap may be locked, while observations are taken only from the eastern part. *Larson and Lisowski* [1994] recently pointed out that there may be a locked patch trenchward of the geodetic network based on the latest observations at the Simeon (SIM) station on Simeonof Island.

With regard to vertical motions, *Beavan et al.* [1984] observed a significant tilt signal based on their short level lines in the same region. With more recent data added, *Beavan* [1992] found that the tilt in the inner Shumagin Islands is 0.10 ± 0.05 μrad/yr trenchward, while tilt in the outer Shumagins is –0.11 ± 0.07 μrad/yr. That is, both the inner and outer Shumagins tilt toward the central part of the group.

Beavan [1992] also found the uplift of Simeon (SIM) relative to Sand Point (SDP); see Figure 2 for locations. He concluded that if the 1976-1991 differential sea level data are interpreted as defining a constant rate of relative motion, then the relative uplift rate is –4.0 ± 1.0 mm/yr, that is, Simeon is subsiding relative to Sand Point. However, if he fit only the higher quality post-1985 data, then the estimated uplift was reduced to –1.8 ± 1.2 mm/yr. Meanwhile, *Savage and Plafker* [1991] analyzed the annual mean sea levels along the south coast of Alaska. After removing the estimated eustatic rate (2.4 ± 0.9 mm/yr) and isostatic rebound (–1.0 ± 0.5 mm/yr), they obtained a marginally significant absolute uplift rate, 2.2 ± 1.2 mm/yr at Sand Point. Hence both the tilt data and uplift data also allow the possibility that the eastern part of the Shumagins gap, where the Shumagin Islands are located, is active and seismically coupled.

Two-Dimensional Finite Element Model

Geometry Definition

A 2-D finite element model (Figure 2) is used to analyze space- and time-dependent stressing in the Shumagins area during earthquake cycles. The model simulates the effects of repeated prior subduction events within the eastern segment of the Shumagin seismic gap. All measurements to which we compare were obtained from islands within that area, and the previous large event of 1917 also originated from the eastern end of the segment and ruptured westward [*Estabrook and Boyd,* 1992].

The 2-D model is clearly an approximation of this region. There are not sufficient data to support a complete three-dimensional simulation. *Beavan et al.* [1984] studied the Shumagins region with a 2-D elastic dislocation model, as did *Savage and Lisowski* [1986] and *Lisowski and Savage* [1988]. The variation of geological structure along the strike in the Shumagin gap does not seem large enough to significantly alter a 2-D description of thrust zone structure, especially for the partially coupled depth range above 50 km. The major concern is the structural boundary in the downgoing plate which *Hudnut and Taber* [1987] pointed out between a western region (which spans 170 km along trench, including part of the 1946 rupture zone and the western part of the Shumagin gap) and an eastern region (about 80 km along trench, including basically all the Shumagin Islands region). The projected cross sections of seismicity show a double seismic zone in the slab only in the western region. However, the variation is most evident below 60 km in depth, and the geometry of the upper surface, as marked by seismicity locations, is basically the same. Because the surface deformation is mostly affected by loading conditions above 50 km and by rheological conditions along or above the upper surface of the subducting slab, we can assume there is no major structural variation in the Shumagins region (about 250 km along trench), and a 2-D approximation of local structure can be justified. Recent work also confirms that the differences occur only in the intermediate and deep areas. The seismicity relocated by *Abers* [1992] reveals the second deeper seismic zone is located only below 75 km. The inverted geometries of the interplate interfaces from both the western and eastern regions [*Reyners and Coles,* 1982] are very close.

Seismicity from a local network shown in depth cross sections by *Reyners and Coles* [1982, Figure 3], *Hauksson* [1985, Figure 9] and *Abers* [1992, Figures 1 and 3] suggest the position of the upper surface of the subducting slab. A notable feature is the change of dip angle at a depth of around 30 km, and one can divide the interplate interface into three parts: an upper shallow dipping part, a rounded transition part, and a lower more steeply dipping part. Similar dip variation can be found based on event locations from the annual seismicity distributions of 1979 and 1981 [*Beavan et al.*, 1984]. Through the latter work we can also determine the location of the interplate interface relative to the islands, as shown in Figure 2. Following the locus of the seismicity, we find the upper part dipping at approximately 10° and the lower part at 32.5°. The bend has been rounded as suggested by, but not closely constrained by, the seismicity locations; this also avoids the spurious stress concentration of a sharp kink.

The extent of the hypothesized locked zone (darkened part of the thin interface region in Figure 2) is also suggested by the seismicity. If we assume the coupled part of the interplate interface will induce more small seismic events in its vicinity than does the uncoupled part, the extent of the locked zone in cross section can be determined from the seismicity distribution of *Hauksson* [1985] and *Abers* [1992]. In this way we think the interplate interface is locked over depths which, when associated to the locations of the nearest nodes of our finite element array, range from 16.7 km to 49.3 km, although the coupling behavior may vary within that range.

To compare, *Reyners and Coles* [1982] argued the plate boundary is brittle to a depth of 45 km because of the microseismicity concentrations in the 25 to 45 km depth range. They thought the inverted thin distribution of seismic events implies a single plane and interpreted it as the interplate interface. *House and Jacob* [1983] assumed shallow seismicity above 60 km to be associated with the brittle portion of the interface. They noticed, from the cross-sectional view of seismicity, that there is a zone of quiescence, at depths from 50 to 60 km, between the shallow- and intermediate-depth earthquakes. The depth of 60 km has been adopted by *Beavan et al.* [1984] to fit tilt data. *Savage and Lisowski* [1986] used 30 km and 50 km, respectively, for their models. Recently, *Abers* [1992] suggested 45 km as the lower bound of the coupled zone because the mechanisms of the $m_b > 6.0$ events indicate a single fault zone plane at 25-45 km depth. *Tichelaar and Ruff* [1993], as part of a global survey, estimated the downdip end of the coupled zone in Alaska based on aftershock zones of large events and distribution of moderate events, $m_b > 6.0$, three in the Shumagins region and two others nearby. They inferred a depth of 37-41 km. *Pacheco et al.* [1993], who also provide a global survey, suggest a depth of 50 km for the eastern Aleutians based on the depth distribution of 21 moderate size events ($5.5 \le M_s \le 7.0$).

Our model has an oceanic plate dipping under an overriding plate, both of which are assumed to respond elastically to stress fluctuation in the earthquake cycle. These are underlain by a mantle and mantle wedge which respond viscoelastically. The effective elastic thickness of the upper plate is taken as 50 km and of the oceanic plate as 30 km. We discuss later effects of varying these thicknesses.

Material Properties

Assumption of a viscoelastic upper mantle and, especially, mantle wedge are considered necessary by some workers to describe a realistic rheology of a subduction zone. For example, *Wahr and Wyss* [1980], in their study of Alaskan earthquakes, pointed out that there is a low Q region below the upper plate which, when interpreted as an anomalously low viscosity volume, provides a plausible fit to their uplift data. Other observations they listed to support the existence of a low-viscosity region include the absence of seismicity, high attenuation of P-waves and poor transmission of S-waves. They assumed a Maxwell viscoelastic volume of very short relaxation time (1 year) in the form of a wedge between the plates extending from 50 to 200 km in depth and 80 km in width, to fit postseismic surface deformation of the 1957 Aleutian earthquake, and a wedge 50 to 80 km in depth and 40 km in width to fit that of the 1964 Alaska earthquake. They proposed the viscoelastic wedgelike zone as an alternative to aseismic creep on the downdip continuation of the fault zone, an approach they argued should be avoided if data can be fit otherwise.

In our modeling, the asthenospheric mantle region below the subducting plate is assumed to be Maxwell viscoelastic with relaxation time $T_{rel} = \eta / \mu$ (η = viscosity, μ = elastic rigidity) that is some fraction of T_{cyc}, where T_{cyc} is the recurrence time of the large underthrusting earthquakes with which we precondition the model up to the 1917 event. We take $T_{cyc} = 70$ years. This T_{rel} is not well constrained but we found suitable fits to the deformation data by taking it as 1/6 to 1/3 of T_{cyc}. Significantly longer values have little effect on results [*Taylor et al.*, this issue], and comparison to observations is mainly controlled by more shallow sources of relaxation. The interplate fault zone is represented by a layer of elements of thickness $h = 1$ km, and we describe below the way in which slip is imposed on the coupled part of that zone. In order to simulate the aseismic response of the shallow fault near the surface of the Earth at the trench, the interplate interface updip from the locked zone (shallower than about 17 km) is defined as a softened viscoelastic material, with rigidity $\mu_{sh} = \mu / 10$ and viscosity $\eta_{sh} = \eta / 20$. These choices are arbitrary but give a representation of the zone such that it does not accumulate large stress from adjoining earthquakes and that it relaxes away whatever stress it does carry in a time that is short compared to T_{cyc}. Also, for T_{rel} as above and $T_{cyc} = 70$ years, the parameters are equivalent to a viscous resistance parameter η_{sh} / h (stress required to maintain unit relative sliding velocity across fault layer) such that $\eta_{sh} / \mu h = 0.6$ to 1.2 yr/km, a range similar to what was found to be consistent with the timing of outer rise seismicity in the Oaxaca, Mexico, subduction zone [*Dmowska et al.*, 1994; see also *Taylor et al.*, this issue].

In order to fit the geodetic data mentioned above, we found that we needed models that substantially relaxed deviatoric stresses over an extensive region beneath or within the mantle wedge, adjacent to the coupled part of the interface. This is similar to the conclusion reached by *Wahr and Wyss* [1980]. Other than the evidence cited above from their work, we have no independent evidence which supports or denies the plausibility of such extensive relaxation on a timescale which is much shorter than the interseismic

period. To deduce the importance of such relaxation, we constructed two groups of models. In the first group we included a rapidly relaxing aseismic fault zone along the interplate interface, as the immediate downdip continuation of the coupled zone. An example is shown as the whitened region in Figure 2, along the 1-km-thick fault layer. This might be justified as approximately representing the thermally based transition from stick-slip to stable shearing and probable loss of strength in dehydrating materials that ultimately supply back arc volcanism. We considered various lengths L of the relaxing region, from 0 to 106 km, and, as will be seen, only the longer ones suitably fit the geodetic data. All these zones start at 50 km depth and the longest, 106 km in length, extends to 106 km depth. In the second group we introduced a rapidly relaxing region that includes a portion of the mantle wedge between the slab and overlying plate. That wedge region is also parameterized by its length L along the slab, downdip from the coupled zone. It occupies a triangular region bounded above by the upper plate and to the right (in Figure 2) by the line of element boundaries running roughly perpendicular to the slab, from the lowest depth of the wedge region along the slab to the base of the upper plate. The largest, which provides the best fit to the data, again has length 106 km along the slab and ranges in depth from 50 to 106 km. This depth might be rationalized because local volcanoes appear to originate from a source at depths of about 100 km [*Jarrard,* 1986]. We found that we needed very short relaxation times in these regions to provide suitable fits to the deformation data.

Let η_f and η_w be the respective viscosities of the aseismic downdip fault and mantle wedge regions discussed. A computational difficulty arises in exploring a large number of models when one or both of the relaxation times η_f / μ and η_w / μ are short. Then the time steps in the calculations, which need to extend over at least one and preferably two or more previous earthquake cycles to sensibly precondition the model, must be made small compared to those relaxation times. We therefore turned to representing such strong relaxation of deviatoric stresses in an approximate manner, as follows. We greatly reduce the elastic rigidity μ_f of the aseismic fault for the first group of models, or μ_w of the portion of wedge region for the second group of models. This means that their small viscosities, η_f or η_w, now correspond to much longer material relaxation times, η_f / μ_f or η_w / μ_w, than those given by η_f / μ or η_w / μ. Thus less extreme reductions of time steps are required. We still keep η_f / μ_f or η_w / μ_w small compared to T_{cyc}, so that deviatoric stresses are well relaxed at the late-cycle times which are of interest for our comparisons to geodetic data. While this procedure is valid for representing late-cycle response in cases of strong relaxation of deviatoric stress, it is important to recognize that what is calculated and shown here as a coseismic response is then inaccurate because of the softened μ_f and/or μ_w. It must really be understood as some combination of the coseismic response and an indeterminate amount of the early postseismic response, over which stresses would relax to a value associated with what is calculated with the reduced rigidity.

For the first group of models, we take $\mu_f = \mu / 100$ within the fault layer of thickness 1 km, and choose the viscosity as follows: We note that the effective system relaxation time for a long and thin viscoelastic faultlike inclusion zone is $T_{rel}^{sys} \approx \eta_f / \mu_f + q\, L\, \eta_f / \mu\, h$, where η_f and μ_f are the viscosity and shear modulus of the inclusion, respectively, μ is the shear modulus of the surrounding material, L and h are characteristic length and thickness of the narrow inclusion, and q is a factor of order unity (strictly, this is true for a narrow ellipsoidal inclusion in an unbounded elastic solid). We thus choose η_f such that, with q = 1, $T_{rel}^{sys} = T_{cyc} / 6$ or $T_{cyc} / 3$, the same as chosen for the mantle regions. With L = 100 km and $T_{rel}^{sys} = T_{cyc} / 6$, this leads to $\eta_f / \mu = T_{cyc} / 1200$, but keeps the material relaxation time, η_f / μ_f, 100 times longer. That allows time steps in the computations to be 100 times larger, hence reducing computer time for a given model to 1% of what would otherwise be required.

A corresponding approximation is made for the strongly relaxing part of the mantle wedge in the second group of models. There we choose $\mu_w = \mu / 10$, and choose η_w such that $\eta_w / \mu_w = T_{cyc} / 12$ or $T_{cyc} / 6$, that is, half of the relaxation time for the rest of the mantle, which is $T_{rel} = T_{cyc} / 6$ or $T_{cyc} / 3$, respectively. Thus the strongly relaxing fore-wedge has $\eta_w / \mu = T_{cyc} / 120$ or $T_{cyc} / 60$, for the respective cases. When T_{cyc} = 70 years as here, these η_w / μ are in the same range as adopted by *Wahr and Wyss* [1980].

Loading

To discuss the loading condition, we introduce the "seismic coupling factor" α, defined as the ratio of seismic slip to the total slip over a cycle in the preconditioning sequence up to, and including, 1917. It is introduced to allow for the large discrepancy between slip rates determined from a global plate model and seismic slip rates from moment summations for several subduction zones. *Pacheco et al.* [1993] have phenomenologically related α to the following parameters: (1) variations in plate convergence rate and age of the downgoing oceanic lithosphere; (2) absolute velocity of the overriding plate in a hotspot reference frame; and (3) differences in the evolutionary stage of subduction. Physically, they relate it to the following: (1) size and distribution of asperities, that is, subregion of large moment release; (2) sediment subduction; and (3) differences in the frictional behavior of materials at the plate interface. They estimated the seismic coupling factor α for 19 subduction zones by summing up the seismic moments within the previous 90 years and also by using the slip-predictable recurrence model for large earthquakes. For most subduction zones, α values obtained by both methods are much smaller than 100%, which suggests unevenly locked seismic coupling zones on the interplate interface.

We can make an a priori estimation of α, independently of our use of the model to fit deformation data. To estimate α, we adopt $M_o = 1.7 \times 10^{20}$ N m for the 1917 event [*Estabrook and Boyd,* 1992], and we choose shear modulus μ as 3.0×10^{10} Pa, average recurrence time T_{cyc} for prior events as 70 years, relative convergent rate V_{pl} as 64 mm/yr, and rupture area 8400 km^2 (for the 97.6-km downdip coupled width in our model, that corresponds to length 86.4 km along strike). This gives a seismic coupling factor α = 0.15. *Estabrook and Boyd* [1992] suggested a rupture length of 75 km and downdip width 100 km, which would result in α = 0.17. A slightly larger α may be justified if the 1917 event was also preceded by a period of accelerating moment release like that shown for the region since approximately 1980 [*Dmowska and Lovison-Golob,* 1991; *Jaumé and*

Estabrook, 1992; *Bufe et al.,* 1994]; we shall see that a larger value, $\alpha = 0.20$, enables a good fit of model results to the deformation data.

These are average α values; as noted, α may vary with depth along the coupled interplate interface. Both *Reyners and Coles* [1982] and *Abers* [1992] have suggested that the main thrust zone is within a 25-45 km depth range. Our attempts to fit geodetic observations also lead us to conclude that the coupling should be stronger in the lower part. We describe the variations by assigning different seismic coupling factors. The ratio of α is 1:1.5:2 along the shallow-dipping part, the transition bend, and the lower more steeply dipping part of the coupled zone. Results associated with area weighted average seismic coupling factors $\alpha = 0.15$ and 0.20 are reported here. Thus when the average $\alpha = 0.20$, the local $\alpha = 0.14$ along the 55.3-km shallow-dipping length of the coupled interface, 0.21 along the 10.7 km curved portion, and 0.28 along the final 35.8 km length of steeply dipping coupled interface.

The coupled part of the interplate interface undergoes periodically repeated large slips $\alpha V_{pl} T_{cyc}$ in the preconditioning period; here α is the local value. As a simplification, but one that has no fundamental basis, we assume that the remaining part $(1 - \alpha) V_{pl} T_{cyc}$ of the total convergence $V_{pl} T_{cyc}$ in a cycle is accommodated by sliding at the constant rate $(1 - \alpha) V_{pl}$. Thus that is the imposed sliding rate along the coupled interface for our modeling of deformations since 1917. This simplifies, in a way suitable for a 2-D model, a distribution of coupling strength, creep, and smaller level seismic events which are likely to be highly heterogeneous along the interface both downdip and along strike, and ignores deviations from uniformity in time of the slip rate in this "aseismic" part of the slippage. The preconditioning slip history (up to and including 1917) is expressed as

$$\Delta u = (1 - \alpha)V_{pl}t + \{1/2 + [t/T_{cyc}]\}\alpha V_{pl}T_{cyc} \qquad (1)$$

where Δu is the slip, t the time, and $[t/T_{cyc}]$ is a staircase function which denotes the integer part of its argument, t/T_{cyc} (Figure 3).

It is convenient to separate the slip into two parts [*Dmowska et al.,* 1988; *Taylor et al.,* this issue]: the steady slip and perturbation slip, as $\Delta u = \Delta u_{steady} + \Delta u_{perturb}$ with $\Delta u_{steady} = V_{pl}t$ and

$$\Delta u_{perturb} = \{1/2 + [t/T_{cyc}] - t/T_{cyc}\}\alpha V_{pl}T_{cyc} \qquad (2)$$

where $\Delta u_{perturb}$ averages, in time, to zero over one whole seismic cycle, and is only associated with the temporal variation of coupling. It drives the time dependencies of stress and deformation which can be monitored by seismicity and geodetic observations. It is this latter part of slip, in (2) and as shown in Figure 3, that has been imposed kinematically onto the coupled part of the interplate interface to determine the time dependence of stress and deformation. As explained by *Dmowska et al.* [1988] and *Taylor et al.* [this issue] in subduction modeling, such a procedure lets us calculate the fluctuating part of the stress, strain, and displacement rate fields. Those fluctuating parts are to be superposed on temporally uniform long-time average stress and velocity fields that are not determined by this type of perturbation analysis. The perturbation slip $\Delta u_{perturb}$ is imposed by writing the shear strain in coupled fault elements as the sum of the usual elastic strain, that is, stress/μ, plus a "transformation" strain which is forced to have the time history $\Delta u_{perturb}/h$. We use the finite element program ABAQUS (made available under academic license from Hibbitt, Karlsson and Sorensen, Inc., of Pawtucket, Rhode Island) for the calculations, and adapt the anisotropic thermal strain procedures within that program to describe purely shear transformation strains, as given by *Rice and Stuart* [1989] and *Taylor et al.* [this issue].

Discussion of Model Results

Numerical predictions of the models in the first group, with a strongly relaxing aseismic continuation of the coupled fault zone extending 106 km downdip, are presented in Figure 4. This case is for coupling factor $\alpha = 0.20$ and mantle (including mantle wedge) relaxation time $T_{rel} = T_{cyc} / 6 = 11.7$ years. Comparisons with data from the deformation observations are also shown in the figure. Table 1 summarizes predicted parameters which can be compared to the deformation data for the four models of this group, with $L = 106$ km, generated with $\alpha = 0.15$ and 0.20, and with $T_{rel} = T_{cyc} / 6$ and $T_{cyc} / 3 = 23.3$ years.

All of the models summarized in Table 1 are in suitable accord with the geodetic observations. There are two estimates of the uplift rate of SIM relative to SDP. If we attempt to fit the first, -4.0 ± 1.0 mm/yr, there is a slight preference for the model with $\alpha = 0.20$ and $T_{rel} = T_{cyc} / 6$. We have not found a model which provides a similarly close fit to the second, -1.8 ± 1.2 mm/yr, but a model with $T_{rel} = T_{cyc} / 3$ and α perhaps slightly reduced from 0.20 might then be slightly preferred.

Table 2 shows predictions of models in this first group for various values of L, from 0 to 106 km. All of these models, except for the second of the two listed with $L = 106$

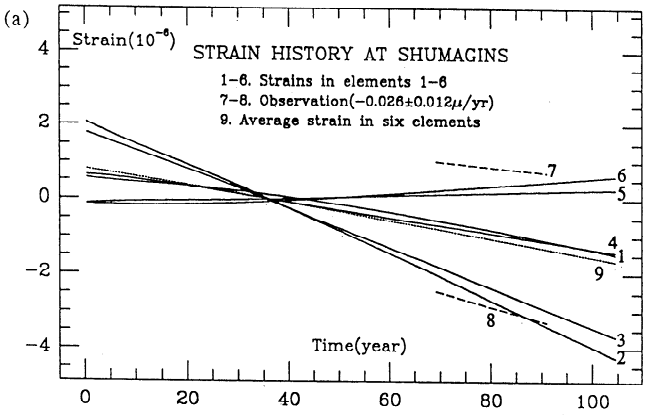

Figure 4a. Numerical results up to 105 years after the 1917 event (cyclic events with $T_{cyc} = 70$ pre-condition the system up to 1917), for model of Figure 2 with seismic coupling factor $\alpha = 0.20$, Maxwell relaxation time $T_{rel} = T_{cyc} / 6 = 11.7$ years in mantle regions, and 106-km-long strongly relaxing aseismic downdip continuation of coupled fault zone, with $\mu_f = \mu / 100$ and $\eta_f / \mu = T_{cyc} / 1200 = 0.06$ year: Solid lines 1 to 6 show surface extensional strain history for the six elements within the network; dotted line 9 shows average over network (numbers identified in Figure 2), and slope is to be compared to that of short-dashed lines 7 and 8 which give bounds based on EDM/GPS strain data.

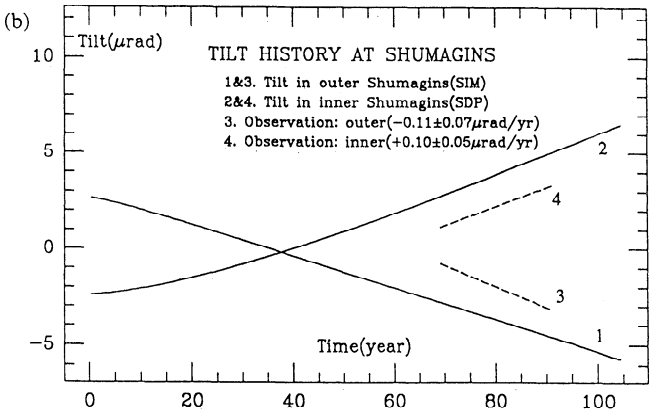

Figure 4b. Tilt in outer and inner Shumagins compared to observations for same period and model as in Figure 4a.

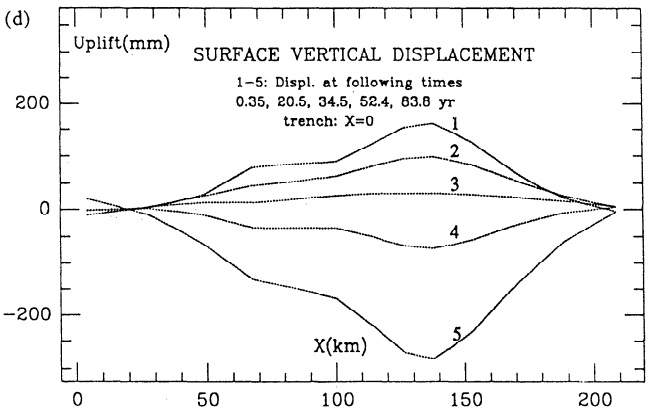

Figure 4d. Vertical displacement profiles predicted for same model as in Figure 4a, at various times since the 1917 event.

km, are for the standard case $\alpha = 0.20$ and $T_{rel} = T_{cyc} / 6$. It is seen that the long length of the relaxing zone is required for reasonable agreement with the estimate of absolute uplift rate at Sand Point and the tilt rate in the outer Shumagins. The second entry with $L = 106$ km shows that the fit degrades somewhat when we do not allow any relaxation in the mantle wedge, outside and above the aseismic fault zone.

Results for the second group of models, with the strongly relaxing fore-wedge region in the mantle, are summarized in Table 3. These are also all for $\alpha = 0.20$ and $T_{rel} = T_{cyc} / 6$ for the rest of the mantle. The second case with length of 106 km along the slab shows the effects of more extreme softening, with both μ_f and η_f reduced by another factor of 10 from the standard case described earlier for this group of models. This more extreme softening does not have a very significant effect. For a given length along the slab of the strongly relaxing part of the wedge, the results for the second group are not very different from the result for models of the first group (as summarized in Table 2). Thus we cannot say precisely where the relaxation should take place, that is, as a narrow interface zone or spread throughout the wedge, to allow agreement with the observations. It does seem that the relaxation has to be strong and to extend on the order of 100 km downdip from the base of the coupled zone.

The effects of the effective elastic thicknesses of the oceanic plate and upper plate were also investigated. All models belong to the first group with a strongly relaxing aseismic continuation up to 106 km in depth downdip from the coupled fault zone, and for the standard case $\alpha = 0.20$ and $T_{rel} = T_{cyc} / 6$. Numerical predictions are summarized in Table 4 and Table 5. We found that the effective elastic thickness of the oceanic plate has very little influence on deformations within the network (Table 4). One reason is

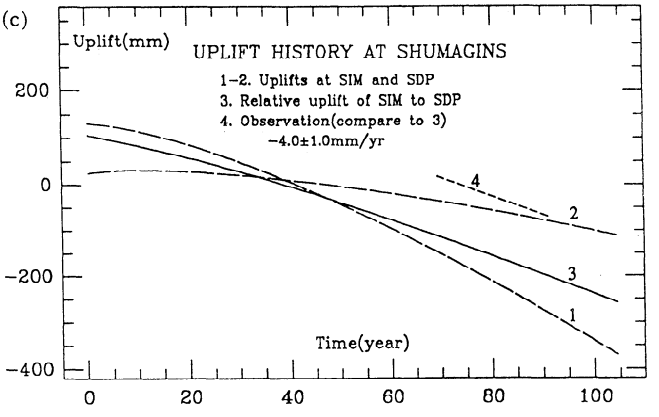

Figure 4c. Uplift at SIM and SDP for same period and model as in Figure 4a, lines 1 and 2; slope of relative uplift in line 3 to be compared to slope of short-dashed line 4 representing observed rate (see footnote c for Table 1).

Table 1. Computation of 2-D Finite Element Modeling and Observations

Deformation Parameters	Model Predictions $\alpha = 0.15$	Model Predictions $\alpha = 0.20$	Observations
For $T_{rel} = T_{cyc} / 6$			
Strain, μstrain/yr			
Averaged over network[a]	−0.018	−0.025	−0.026 ± 0.012
Tilt, μrad/yr			
Inner Shumagins[b]	0.078	0.104	0.10 ± 0.05
Outer Shumagins[b]	−0.062	−0.083	−0.11 ± 0.07
Uplift, mm/yr			
SIM relative to SDP[c]	−3.1	−4.1	−4.0 ± 1.0[c]
SDP absolute[d]	−1.5	−2.0	−2.2 ± 1.2
For $T_{rel} = T_{cyc} / 3$			
Strain, μstrain/yr			
Averaged over network[a]	−0.019	−0.026	−0.026 ± 0.012
Tilt, μrad/yr			
Inner Shumagins[b]	0.070	0.093	0.10 ± 0.05
Outer Shumagins[b]	−0.062	−0.083	−0.11 ± 0.07
Uplift, mm/yr			
SIM relative to SDP[c]	−2.6	−3.5	−4.0 ± 1.0[c]
SDP absolute[d]	−1.3	−1.7	−2.2 ± 1.2

[a]From *Larson and Lisowski* [1994], combining results of GPS survey for 1987-1991 and earlier [*Lisowski et al.*, 1988] EDM survey for 1980-1987.

[b]From *Beavan* [1992], tilt measurement, for 1981-1991.

[c]From *Beavan* [1992], based on sea level data: if the 1976-1991 differential sea level data are interpreted as constant tilt rate, then SIM appears to be subsiding relative to SDP at 4 ± 1 mm/yr; if, however, the fit is made only to higher quality post-1985 data, then SIM is subsiding relative to SDP at 1.8 ± 1.2 mm/yr.

[d]From *Savage and Plafker* [1991], based on sea level change (1970-1990), adjusted to account for postglacial rebound rate and eustatic rate.

Table 2. Strongly Relaxing Aseismic Fault Zone, of Length Indicated, Along Interplate Interface Downdip from Seismically Coupled Zone

Length, Aseismic Fault, km	Strain Rate EDM/GPS, μstrain / yr	Tilt Rate Inner, μrad / yr	Tilt Rate Outer, μrad / yr	Uplift Rate Relative, SIM–SDP, mm / yr	Uplift Rate Absolute, SDP, mm / yr
0[a]	− 0.0157	0.084	− 0.039	− 5.63	0.31
14[a]	− 0.0158	0.086	− 0.047	− 5.61	0.30
29[a]	− 0.0184	0.099	− 0.057	− 5.50	− 0.10
45[a]	− 0.0208	0.108	− 0.067	− 5.21	− 0.62
64[a]	− 0.0227	0.109	− 0.072	− 4.79	− 1.15
84[a]	− 0.0239	0.107	− 0.077	− 4.42	− 1.64
106[a]	− 0.0245	0.104	− 0.083	− 4.09	− 2.02
106[b]	− 0.0205	0.088	− 0.077	− 3.85	− 1.63
Data	− 0.026 ± 0.012	0.10 ± 0.05	− 0.11 ± 0.07	− 4.0 ± 1.0[c]	− 2.2 ± 1.2

[a]Aseismic downdip fault zone has $\mu_f = \mu / 100$, η_f chosen so that $T_{rel}^{sys} = T_{cyc} / 6$, and $h = 1$ km; viscoelastic mantle, including mantle wedge, with $T_{rel} = \eta / \mu = T_{cyc} / 6$; $\alpha = 0.20$.
[b]Same as case above, except that now mantle is viscoelastic only below the subducting plate, and the mantle wedge is elastic.
[c]See footnote c, Table 1.

the long distance between the network and the area where material properties have been changed. A second reason is the strongly relaxing aseismic zone in the middle, which attenuates stress redistribution induced by a thinner or thicker oceanic plate. The effective elastic thickness of the upper plate, however, has a more significant influence on results (Table 5). The relatively shorter distance between the network and the adjusted area is thought to be the reason. Still, variation over the 43 to 58 km region shown does not seriously misfit the data. We have adjusted the extent of the coupled fault zone so that its lower end always coincides with the bottom of the upper plate, and we have rescaled the local α values (keeping the 1:1.5:2 ratio) so that the total moment release in each preconditioning event is the same as for the standard model with 50 km thickness. This reflects a hypotheses that the seismically coupled zone should be coincident with the brittle layer of the upper plate.

We build our viscoelastic model with geometric parameters constrained by seismicity in the Shumagins region and the general understanding of mechanical and thermal structure at subduction zones. *Beavan et al.* [1984] used a partial coupling elastic model to study the same area. They postulated that a 0.8-m dislocation propagates up from a depth of 80 km to 20 km along a 32° dipping plane to fit anomalous tilt data during 1978-1980 and suggested that such events can be a regular process at subduction zones. If the propagation process took more than 2 years to finish, the induced strain rate on the Earth's surface in the Shumagins region would not be resolvable. While such aseismic events may be episodic, our model treats them as contributing to the slip rate $(1 - \alpha) V_{pl}$ which is taken as uniform in time. Even though the profile of the interplate interface is similar, our models differ from the *Beavan et al.* [1984] model and other elastic models in the following aspects: (1) Material properties: The viscosity in the aseismic fault zones and mantle wedge is crucial in fitting the geodetic data. (2) Observations: Our modeling is constrained not only by tilt data, but also by strain and uplift data. (3) Loading condition: *Beavan et al.* [1984] assumed that a large event will occur along the shallow part (above 20 km) and that the lower part undergoes a series of episodic aseismic events such as the one inferred during 1978-1980. We assume that the lower part of the thrust zone (20 - 49 km in depth) is more seismically coupled while the upper part (16 - 20 km in depth) is less coupled.

Savage and Lisowski [1986] also used the elastic dislocation model to predict strain rates in the Shumagins region, as discussed earlier, and found the predicted results (for $\alpha = 1$) were about an order of magnitude higher than the data. They also mentioned that a viscoelastic model, which for them consisted of an elastic layer (the lithosphere) resting upon a viscoelastic half-space (the asthenosphere), was compatible with smaller strain rates if the seismogenic

Table 3. Strongly Relaxing Mantle Wedge Region, Coinciding with Length Indicated Along Top of Slab, and Extending Upward to Base of Overlying Plate

Length Along Slab, km	Strain rate EDM/GPS, μstrain / yr	Tilt rate Inner, μrad / yr	Tilt rate Outer, μrad / yr	Uplift rate Relative, SIM–SDP, mm / yr	Uplift rate Absolute, SDP, mm / yr
64[a]	− 0.0241	0.118	− 0.083	− 4.88	− 1.26
106[a]	− 0.0260	0.112	− 0.088	− 4.18	− 2.10
106[b]	− 0.0280	0.111	− 0.093	− 3.77	− 2.53
Data	− 0.026 ± 0.012	0.10 ± 0.05	− 0.11 ± 0.07	− 4.0 ± 1.0[c]	− 2.2 ± 1.2

[a]Fore-wedge region has $\mu_w = \mu / 10$, $\eta_w / \mu_w = T_{cyc} / 12$; rest of mantle has $T_{rel} = \eta / \mu = T_{cyc} / 6$; $\alpha = 0.20$.
[b]For μ_w and η_w reduced by further factor of 10 from previous case.
[c]See note c, Table 1.

Table 4. Oceanic Plate, with Effective Elastic Thickness Indicated, Above Mantle, and Beneath Upper Plate and Mantle Wedge

Effective Thickness, km	Strain rate EDM/GPS, μstrain / yr	Tilt Rate Inner, μrad / yr	Tilt Rate Outer, μrad / yr	Uplift Rate Relative, SIM–SDP, mm / yr	Uplift Rate Absolute, SDP, mm / yr
22.5	−0.0239	0.101	−0.083	−4.03	−2.01
30.0	−0.0245	0.104	−0.083	−4.09	−2.02
40.7	−0.0256	0.104	−0.083	−3.91	−2.10
52.4	−0.0268	0.104	−0.088	−3.62	−2.18
Data	−0.026 ± 0.012	0.10 ± 0.05	−0.11 ± 0.07	−4.0 ± 1.0[a]	−2.2 ± 1.2

[a]See footnote c, Table 1.

fault zone cuts through lithosphere, and asthenosphere relaxation time is short compared with earthquake recurrence time. We think a more realistic viscoelastic model is one with an elastic slab that penetrates the asthenosphere, with possibly different relaxation behavior in the wedge region above the slab.

We investigated other model possibilities in this work, such as different geometries of the interplate interface and different locking depth terminations updip. It was observed that the stressing and deformation on the surface of the Earth are sensitive to the details of location of the thrust interface. Our models, as constrained by seismicity, include two dip angles, one for the shallow part and the other for the intermediate part of the slab. If the two slab segments form a corner, the spurious stress concentration there significantly affects surface deformation and uplift. Even with a smooth bend, the results are sensitive to the radius of curvature, and a larger radius will result in more uniform deformation on the surface. Features of the vertical displacement profile (Figure 4d) are controlled by this geometry and also by the distribution of the coupling factor α. Our modeling shows that the pattern of vertical displacement at the surface, with the position of late-cycle subsidence shifted away from the trench, is a direct result of the two dip angles of the subducting slab. In a model with smaller local α within the downdip part of the coupled zone, we observed smaller late-cycle vertical displacement rates within the network.

Conclusions

Our approach in this work has been to assume that the Shumagins region is seismically coupled and to use seismicity data to constrain, within a 2-D model, the overall coupling factor α, the approximate recurrence interval T_{cyc} of previous events (up to 1917), the location of the thrust interface, and the extent of the coupled region along it. We have then adjusted the distribution of the coupling factor, viscosity of the mantle, and locations of more strongly relaxing regions (along the downdip continuation of the interface or in the fore-wedge) to find models that are consistent with the surface strain, tilt and uplift observations. Coupled models of a type that would produce repeated earthquakes with parameters similar to the 1917 event have been identified that are consistent with the deformation data. All such models involve significant relaxation over an extensive region of the mantle wedge or along an aseismic downdip continuation of the coupled interface. We have no independent evidence for such relaxation, other than the factors cited by *Wahr and Wyss* [1980] and summarized earlier here. We cannot pick a unique model from a set of significantly coupled models with α near to 0.20; any of several succeed in matching the geodetic results. It is evident, however, that either from our approach or a conventional purely elastic model, the assumption that the Shumagins region is not presently coupled (i.e., that $\alpha = 0$) would predict zero strain, tilt and uplift rates, and therefore would not be similarly compatible with the deformation data.

Using the preferred $\alpha = 0.20$, and recalling that $\alpha = 0.15$ to 0.17 characterizes a 1917 event ($M_o = 1.7 \times 10^{20}$ N m) every 70 years, our modeling suggests that the eastern region of the Shumagin gap has accumulated seismic moment during the current loading episode at a rate of approximately 2.1×10^{20} N m per 70 yr, so that 2.3×10^{20} N m must be accounted for by mid-1995. The May 13, 1993, $M_s = 6.9$ event in the Shumagin region released 0.2-0.3 $\times 10^{20}$ N m and ruptured 43 km along strike and 14 km width in the lower part of the coupled zone assumed here [*Lu et al.*, 1994; *Tanioka et al.*, 1994]. That event may plausibly

Table 5. Upper Plate, with Effective Elastic Thickness Indicated, Above Subducting Plate and Mantle Wedge

Effective Thickness, km	Strain Rate EDM/GPS, μstrain / yr	Tilt Rate Inner, μrad / yr	Tilt Rate Outer, μrad / yr	Uplift Rate Relative, SIM–SDP, mm / yr	Uplift Rate Absolute, SDP, mm / yr
43.1	−0.0256	0.099	−0.069	−5.41	−1.30
50.0	−0.0245	0.104	−0.083	−4.09	−2.02
57.6	−0.0233	0.095	−0.082	−2.86	−2.58
Data	−0.026 ± 0.012	0.10 ± 0.05	−0.11 ± 0.07	−4.0 ± 1.0[a]	−2.2 ± 1.2

[a]See footnote c, Table 1.

be interpreted as a part of the rupture process that will terminate the current loading episode, but it corresponds to release of only about 7-10 years of moment accumulation, that is, to 9-13% of the moment accumulated from 1917 to 1993. Moment release in thrust events over the entire Shumagin gap, in the period of accelerated release discussed earlier, summed to about 0.3-0.4 $\times$ 10^{20} N m from the late 1970s to before that 1993 event [*Dmowska and Lovison-Golob,* 1991; *Jaumé and Estabrook,* 1992], and perhaps half of that could be allotted to the eastern portion. So we can account for only a small part of the estimated mid-1995 moment. Thus we suggest that there is an accumulated moment over the 1917 rupture zone of approximately 1.9 $\times$ 10^{20} N m which has not been released as of mid-1995, and that it will be released in one or more significant earthquakes in the Shumagin Islands region.

Acknowledgments. This study was initiated under support of NSF grant EAR-90-04556 and completed under support of USGS through NEHRP grant 1434-93-G-2325. We are grateful for discussions with G. Abers, J. Beavan, K. M. Larson, M. Lisowski, J. C. Savage, and W. D. Stuart, and for thoughtful comments on the original manuscript by J. Beavan, K. Hudnut, and M. Lisowski.

References

Abers, G. A., Relationship between shallow- and intermediate-depth seismicity in the eastern Aleutian subduction zone, *Geophys. Res. Lett., 19,* 2019-2022, 1992.

Beavan, J., Crustal deformation measurements in the Shumagins seismic gap, Alaska, *U. S. Geol. Surv. Open-File Rep. 92-258,* 145-150, 1992.

Beavan, J., R. Bilham, and K. Hurst, Coherent tilt signals observed in the Shumagin seismic gap: Detection of time-dependent subduction at depth?, *J.Geophys. Res., 89,* 4478-4492, 1984.

Bufe, C. G., S. P. Nishenko, and D. J. Varnes, Seismicity trends and potential for large earthquakes in the Alaska-Aleutian region, *Pure Appl. Geophys., 142,* 83-99, 1994.

Davies, J., L. Sykes, L. House, and K. Jacob, Shumagin seismic gap, Alaska Peninsula: History of great earthquakes, tectonic setting, and evidence for high seismic potential, *J. Geophys. Res., 86,* 3821-3855, 1981.

Dmowska, R., and L. C. Lovison-Golob, Stress transfer and seismic phenomena in the Shumagin Islands region, Alaska (abstract), *Eos Trans. AGU, 72* (44), Fall Meet. Suppl., 322, 1991.

Dmowska, R., J. R. Rice, L. C. Lovison, and D. Josell, Stress transfer and seismic phenomena in coupled subduction zones during the earthquake cycle, *J. Geophys. Res., 93,* 7869-7884, 1988.

Dmowska, R., G. Zheng, and J. R. Rice, Rheological and tectonic controls on stressing history and seismicity in the outer-rise during the earthquake cycle: Oaxaca 1978, Mexico, Segment, (abstract), *Eos Trans. AGU, 75* (44) , Fall Meet. Suppl., p. 449, 1994.

Estabrook, C. H., and T. M. Boyd, The Shumagin Islands, Alaska, earthquake of 31 May 1917, *Bull. Seismol. Soc. Am., 82,* 755-773, 1992.

Estabrook, C. H., K. H. Jacob, and L. R. Sykes, Body wave and surface wave analysis of large and great earthquakes along the Eastern Aleutian Arc, 1923-1993: Implications for future events, *J. Geophys. Res., 99,* 11643-11662, 1994.

Hauksson, E., Structure of the Benioff zone beneath the Shumagin Islands, Alaska: Relocation of local earthquakes using three-dimensional ray tracing, *J. Geophys. Res., 90,* 635-649, 1985.

House, L. S., and K. H. Jacob, Earthquakes, plate subduction, and stress reversals in the eastern Aleutian arc, *J. Geophys. Res., 88,* 9347-9373, 1983.

Hudnut, K. W., and J. J. Taber, Transition from double to single Wadati-Benioff seismic zone in the Shumagin Islands, Alaska, *Geophys. Res. Lett., 14,* 143-146, 1987.

Jarrard, R. D., Relations among subduction parameters, *Rev. Geophys., 24,* 217-284, 1986.

Jaumé, S. C. and C. H. Estabrook, Accelerating moment release and outer-rise compression: Possible precursors to the next great earthquake in the Alaska Peninsula region, *Geophys. Res. Lett., 19,* 345-348, 1992.

Kelleher, J. A., Space-time seismicity of the Alaska-Aleutian seismic zone, *J. Geophys. Res., 75,* 5745-5756, 1970.

Larson, K. M., and M. Lisowski, Strain accumulation in the Shumagin Islands: Results of initial GPS measurements, *Geophys. Res. Lett., 21,* 489-492, 1994.

Lisowski, M., J. C. Savage, W. H. Prescott, and W. K. Gross, Absence of strain accumulation in the Shumagin seismic gap, Alaska, 1980-1987, *J. Geophys. Res., 93,* 7909-7922, 1988.

Lu, Z., M. Wyss, G. Tytgat, S. McNutt, and S. Stihler, Aftershocks of the 13 May 1993 Shumagin, Alaska, earthquake, *Geophys. Res. Lett., 21,* 497-500, 1994.

Nishenko, S. P., Circum-Pacific seismic potential: 1989-1999, *Pure Appl. Geophys., 135,* 169-259, 1991.

Pacheco, J. F., L. R. Sykes, and C. H. Scholz, Nature of seismic coupling along simple plate boundaries of the subduction type, *J. Geophys. Res., 98,* 14133-14159, 1993.

Reyners, M., and K. S. Coles, Fine structure of the dipping seismic zone and subduction mechanics in the Shumagin Islands, Alaska, *J. Geophys. Res., 87,* 356-366, 1982.

Rice, J. R., and W. D. Stuart, Stressing in and near a strongly coupled subduction zone during the earthquake cycle (abstract), *Eos Trans. AGU, 70,* 1063, 1989.

Savage, J. C., A dislocation model of strain accumulation and release at a subduction zone, *J. Geophys. Res., 88,* 4984-4996, 1983.

Savage, J. C., and M. Lisowski, Strain accumulation in the Shumagin seismic gap, Alaska, *J. Geophys. Res., 91,* 7447-7454, 1986.

Savage, J. C., and G. Plafker, Tide gage measurements of uplift along the south coast of Alaska, *J. Geophys. Res., 96,* 4325-4335, 1991.

Sykes, L. R., and S. C. Jaumé, Seismic activity on neighbouring faults as a long-term precursor to large earthquakes in the San Francisco Bay area, *Nature, 348,* 595-599, 1990.

Tanioka, Y., K. Satake, L. Ruff, and F. Gonzalez, Fault parameters and tsunami excitation of the May 13, 1993, Shumagin Islands earthquake, *Geophys. Res. Lett., 21,* 967-970, 1994.

Taylor, M. A. J., G. Zheng, J. R. Rice, W. D. Stuart, and R. Dmowska, Cyclic stressing and seismicity at strongly coupled subduction zones, *J. Geophys. Res.*, this issue.

Tichelaar, B. W., and L. J. Ruff, Depth of seismic coupling along subduction zones, *J. Geophys. Res., 98,* 2017-2037, 1993.

Wahr, J., and M. Wyss, Interpretation of postseismic deformation with a viscoelastic relaxation model, *J. Geophys. Res., 85,* 6471-6477, 1980.

R. Dmowska, J. R. Rice, and G. Zheng, Division of Applied Sciences, and Department of Earth and Planetary Sciences, Harvard University, 323 Pierce Hall, 29 Oxford Street, Cambridge, MA 02138. (e-mail: zheng@gems.harvard.edu)

(Received April 17, 1995; revised October 20, 1995; accepted November 9, 1995)